Deep physico-chemical characterization of individual serum antibody responses against SARS-CoV-2 RBD using a dual titration microspot assay

Ágnes Kovács[1,2], Zoltán Hérincs[3*], Krisztián Papp[3*], Jakub Zbigniew Kaczmarek[4], Daniel Nyberg Larsen[4,5], Pernille Stage[4], László Bereczki[6], Eszter Ujhelyi[6], Tamás Pfeil[2,7], József Prechl[3]*

1 Department of Biostatistics, University of Veterinary Medicine Budapest, H-1078 Budapest, Hungary
2 Department of Applied Analysis and Computational Mathematics, Eötvös Loránd University, H-1117 Budapest, Hungary
3 R&D Laboratory, Diagnosticum Zrt, H-1047 Budapest, Hungary
4 Ovodan Biotech A/S, DK-5000 Odense, Denmark
5 University of Southern Denmark, DK-5230 Odense, Denmark
6 G1 Labordiagnosztikai Kft, H-1036 Budapest, Hungary
7 ELKH-ELTE Numerical Analysis and Large Networks Research Group, H-1117 Budapest, Hungary

*These authors contributed equally.

Abstract

Antigen specific humoral immunity can be characterized by the analysis of serum antibodies. While serological assays for the measurement of antibody levels and of neutralization potential against SARS-CoV-2 are available, these are not quantitative in the biochemical sense. Yet, understanding the biology of COVID-19 would need an unambiguous, complete, quantitative, comparable measurement of specific serum antibodies.
Here we describe a fluorescent, dual-titration immunoassay, which provides the physico-chemical parameters that are both necessary and sufficient to quantitatively characterize the humoral immune response. We used recombinant Receptor Binding Domain of SARS-CoV-2 as antigen on microspot arrays and varied the concentration of both the antigen and serum antibodies from vaccinated persons to obtain a measurement matrix of binding data. Binding curves were fitted using a novel algorithm to obtain thermodynamic variables of binding. We defined the standard state for a system of serum antibodies and antigen and showed how a normalized generalized logistic function is related to thermodynamic activity, standard concentration and activity coefficient. The utility of the method is demonstrated by defining the composition of tested sera with respect to immunoglobulin classes, affinity, concentration, and thermodynamic activity.
The proposed fluorescent dual-titration microspot immunoassay can generate truly quantitative serological data that is suitable for immunological, medical and systems biological analysis.

Keywords: antibody, serology, microarray, physical chemistry, thermodynamics, curve fitting, SARS-CoV-2, quantitative systems biology, Richards function

1. Introduction

The adaptive immune system maintains host integrity by controlling the levels of molecules and cells over a very wide range. The humoral adaptive immune system achieves this by employing effector molecules with tunable specificity and efficiency. These molecules, antibodies, evolve with the help of B lymphocytes that employ them both as sensors for their survival and as effectors for the removal of target molecules. To protect against viral invasion of host cells, antibodies with enhanced effector activity (1) are produced and persist (2). However, the emergence of novel viruses with enhanced ability to enter and spread in the host may overwhelm before such responses might take place (3). Vaccination can prime immune responses and thereby mitigate or evade viral invasion of host cells by inducing the expansion and differentiation of pathogen specific cells. Since antibodies circulating in blood are good indicators of the status of humoral immunity, the characterization of serum antibodies, serology, plays a critical role in immunodiagnostics.

Currently two main approaches dominate serological methods of COVID specific antibody measurements: titration and single-point assays. Titration is the use of a series of gradually diluted serum and the determination of mid-point or end-point from the dilution curve. This approach does incorporate the measurement of effects due to changing reaction conditions, but the readout most often neglects curve shape and focuses on one parameter: the titer. Single-point measurements are optimized for diagnostic power (sensitivity and specificity) (4–6) and neglect potential effects of serum dilution. The readout of single-point measurements is an arbitrary though standardized unit of reactivity. Virus neutralization (7) and surrogate neutralization assays (8,9) can also be carried out in the single-point or titration format. What is common in these assays is that none of them varies or takes into account the density of the target molecule used in the assay: the solid-phase coupled antigen or the virus receptor on cells.

Infection with SARS-CoV-2 results in the appearance of IgM (10), IgG (11–13) and IgA (14) directed against various viral components (15–18). The response builds on immunological imprints from common cold viruses (19), is connected to disease severity (20–24) and lasts several months (25,26). Vaccination also induces antibody production, therefore serological measurements can help assess vaccine immunogenicity and estimate protectivity (27–30), durability (31) and cross-reactivity with emerging new variants (32). The various indicators of humoral immune response, such as titers (33,34), avidity (35), glycosylation (22) of virus specific antibodies are all related to clinical aspects of the infection and disease, but these relationships are highly variable, not definite (3), partially because of the difficulties in comparing different measurement methods (21).

The physics of molecular interactions is described by physical chemistry and chemical thermodynamics. Interactions between antibody and antigen constitute the basis of immunoassays and several physical and mathematical models have been developed and utilized, but these are primarily assays for antigen and determine antigen concentration. Less attention has been paid to the development of models dedicated to the special requirements of circulating serum antibody detection. Serum antibodies are highly heterogeneous with respect to epitope recognition, affinity, concentrations and structure. A blood serum sample in fact reflects immunological memory of past infections, diseases, along with current immunological activity. While serological assay results are given in units of activity, no clear relationship to thermodynamic activity has been established (36). Early approaches of antigen-antibody interaction modeling, based on predictions of molecular properties (37), similar to current statistical associating fluid theory models, suggested that too many physical properties of the interacting molecules should be estimated.

The difficulty of serum antibody quantification lies in the fact that we are dealing with two unknown variables: affinities and concentrations of antibodies that bind to the Ag in the assay. Any approach aiming to quantify serum antibodies should consider estimating both of these. Lippok et al. used microscale thermopheresis to measure both affinity and concentration of polyclonal antibodies in

solution (38). By titration and competition, they estimated apparent K_D and concentration but no other parameters of distribution. Other approaches mostly focus either on concentration or on affinity. Equilibrium dialysis was the method of choice for measuring affinity constants in solution when radioimmunoassays were used. These assays used a constant concentration of Ab (e.g., 1:100 dilution of serum) and varying concentrations of Ag, calculating the concentration of free radioactively labeled Ag, once equilibrium is established, from the radioactivity. The Scatchard plot was used for calculating the median and mean K_D (39) and for the assessment of affinity heterogeneity and the Sips plot was used for quantifying heterogeneity (40,41).

Rather than focusing on individual molecular properties, we took an approach that examines the resultant physical properties of the system of serum antibodies. We assumed that the deconvolution of thermodynamic activity into quality and quantity, i.e., thermodynamic activity coefficient and concentration, would provide a solution for quantitative serology. We have recently developed a microspot-based, dual-titration immunoassay for the estimation of affinity distribution for multiple immunoglobulin classes (42) utilizing an advanced fitting algorithm (43). Here we describe a further improvement of the assay and its application for the characterization of anti-SARS-CoV-2 antibody response, by the estimation of chemical thermodynamic variables of SARS-CoV-2 RBD specific antibodies of various classes.

2. Methods

2.1 Serum samples

Serum collected from persons working in the laboratory (R&D Laboratory, Diagnosticum Zrt), who volunteered to participate in the serological monitoring of vaccination effects, was used in the study. An informed written consent to take part in the study was obtained from all participants and the study was approved by the institutional ethical review board. Sera were aliquoted and stored frozen until measurement. Participants received vaccines as part of the national vaccination campaign and were randomly chosen for being vaccinated with BNT162b2 (Pfizer-BioNTech), HB02 (Sinopharm) or Gam-COVID-Vac (Sputnik-V). Booster immunizations were carried out as prescribed by the manufacturer.

A commercially available ECLIA test, Elecsys® Anti-SARS-CoV-2 S from Roche for the in vitro quantitative determination of antibodies (including IgG) to the SARS-CoV-2 spike (S) protein receptor binding domain (RBD) in human serum and plasma was used as a reference measurement and was carried out according to the manufacturer's instructions.

2.2.1 Gene synthesis, protein expression and characterization of SARS-CoV-2 Spike RBD 319-541

SARS-CoV-2 Spike RBD 319-541 sequence was based on the first strain of SARS-CoV-2 isolated from a clinical patient on January the 6th 2020, (GISAID: EPI_ISL_402119). The sequence was synthesized to include the Tyr-Pho signal peptide and a N-terminal hexahistidine (6xHIS) tag. The construct was synthesized and cloned commercially into pcDNA3.4-TOPO plasmid (Life Technologies B.V. Europe). SARS-CoV-2 Spike RBD 319-541 recombinant protein (OBA0101, Ovodan Biotech) was expressed in 25 mL culture using the Expi293F expression system (#A14635; ThermoFisher Scientific) according to manufacturer's instructions. Expressed proteins were harvested by centrifugation 6 days post transfection and immediately purified from the supernatant on a Ni-NTA Superflow column (#30430, Qiagen). Eluted protein fraction was buffer exchanged into PBS pH 7.4 using a HiPrep 26/10 Desalting column (#GE17-5087-01, Cytiva) and stored at -20°C. Obtained protein fraction has been subjected to Sodium Dodecyl Sulfate Polyacrylamide gel electrophoresis (SDS-PAGE) using RunBlue (#ab270467 Abcam) 4-12% Bis-Tris polyacrylamide gel. Electrophoresis was performed by using Easy Power 500 (Invitrogen) in a non-reduced environment for 45 minutes at 200V at110mA. Staining was performed

by Coomassie Simply Blue Safe Stain (#LC6060 Invitrogen) and developed according to the manufacturer's instructions.

2.2.2 SARS-CoV-2 recombinant RBD sequence characterization by Mass Spectrometry

A total of 20 µg of SARS-CoV-2 Spike RBD 319-541 was reduced with dithiothreitol (20 mM) for 30 min. at 57 °C and alkylated with iodoacetamide (54 mM) for 20 minutes at RT and in the dark, the reaction was stopped with dithiothreitol. The reduced and alkylated SARS-CoV-2 Spike RBD 319-541 was split into two batches, where the first was treated with trypsin (2%) for 1 hour at 57 °C and PNGaseF (0.5 µl) for 1 hour at 37 °C, while the other was only treated with trypsin (2%) for 1 hour at 57 °C. The two batches were micro-purified prior to analysis by mass spectrometry in accordance with Rappsilber et al. (44). Both batches were run in duplicate with a standard liquid chromatographic tandem mass spectrometric analysis on an Orbitrap ExplorisTM 480 Mass Spectrometer from Thermo Fisher Scientific. The following main settings were used; MS1 resolution: 120000, scan range (m/z): 350-1400, dynamic exclusion after 1 time with an exclusion time of 30 seconds, MS2 resolution: 30000, isolation window MS2 (m/z): 0.8, first mass MS2 (m/z): 110, data type: centroid. The data files from the mass spectrometer were converted using MSConvert from ProteoWizard [https://proteowizard.sourceforge.io/], followed by data search and analysis in GPMAW from Lighthouse Data [http://www.gpmaw.com/]. The mass spectrometry proteomics data have been deposited to the ProteomeXchange Consortium via the PRIDE (45) partner repository with the dataset identifier PXD040415.

Further details of protein characterization are available online as **extended data**.

2.3 Dual-titration microspot immunoassay

Maps of the layout of slides and subarrays, along with description of the protocol are available online as **extended data**.

2.3.1 Microarray production

Experiments were carried out on hydrogel-coated glass slides (Nexterion Slide H, Schott) by using a BioOdyssey Calligrapher MiniArrayer (BioRad). A 14-point dilution series of RBD was prepared with a combination of a ½ and ⅓ diluting series, and spotted on slides in triplicates. The final concentration gradient steps were: 16.66, 8.33, 5.55, 4.16, 2.08, 1.85, 1.04, 0.61, 0.52, 0.26, 0.20, 0.13, 0.068 and 0.065 µM. Slides were dried for 1h at 37°C then soaked in 0.1 M Tris buffer (pH=8.0) for 1h at 37°C in order to block reactive residues on the surface. Once prepared, slides were kept in sealed non-transparent bags at 4°C.

2.3.2 Sample handling and signal detection

Dried arrays were rehydrated in 110 µl PBS (3×5 minutes) before using, then sub-arrays were incubated in 70 µl diluted sample at 37 °C for 1 h. Sample dilution was carried out in PBS-BSA-Tween (PBS, 0.5% BSA, 0.05% Tween 20). Serum treated slides were washed in 0.05% Tween-PBS, then incubated at room temperature for 30 minutes with fluorescently labeled antibodies that were diluted in the blocking buffer (0.05% Tween 20, 2% BSA, PBS). The first mix of detecting antibodies was composed of the following: anti-human-IgG $F(ab')_2$ – Alexa488 (Jackson, Ref.:109-646-097), anti-human-IgA – Alexa647 (Jackson, Ref.:109-606-011), anti-human-IgM – Cy3 (Jackson, Ref.: 109-166-129). In parallel, another microarray was developed with the second detection mix: goat anti-human kappa chain Alexa555 (Southern Biotech, Ref.:2060-32) and goat anti-human lambda chain Alexa647 (Southern Biotech, Ref.: 2070-30). Chips were washed again and following drying, slides were scanned using SensoSpot fluorescent microarray scanner (Sensovation AG, Stockach, Germany).

2.3.3 Analysis of the microarray data

Images of the slides were analyzed with GenePix Pro 6.0 software after visual inspection. Spots were recognized, aligned and analyzed by the program, then gpr files containing the spot data were created. Relative fluorescence intensity (RFI) values were calculated for each spot using the feature's median RFI value of which the feature's local background was subtracted individually for each feature. Further analysis was carried out by using the statistical programming environment R (version 3.5.2).

2.4 Curve fitting

The general theoretical approach to data analysis was similar to that described recently (42).We use a linear model for polyclonal reactions (46) taking into consideration that a bound antibody inhibits nearby free antigens from forming complexes with other antibodies such that the concentration of immune complexes is a logistic function of the logarithm of the total antigen concentration. Since the logarithm of fluorescent intensity is proportional to the logarithm of bound Ab concentration, we assume that the fluorescent intensity of detected antibodies is a Richards function (R) of the logarithm of total antigen concentration (see Supplementary text 1 of (42)), with the following parametrization:

$$R(x) = A * (1 + \nu e^{-k(x-x_i)})^{-\frac{1}{\nu}} \quad (1)$$

with k = 1, where x is logarithm of Ag concentration ln[Ag], A is the signal corresponding to total antibody concentration [Ab] (limit of function R(x) at infinity), x_i is the inflection point of function R, ν is the asymmetry parameter.

The upper limit of the fluorescence, A, depends on the dilution of serum: the less diluted the serum sample, the higher the Ab concentration. We used the reciprocal of serum dilution as a surrogate Ab concentration. Ten times diluted serum corresponds to a concentration of 0.1. The fluorescent signal intensity of bound Ab is thus determined by both Ag and Ab concentrations, which we express using the logarithm total antigen concentration, x=ln[Ag], and the logarithm of the reciprocal of serum dilution factor, y=ln[Ab], as the product of two generalized logistic functions ($R_1(x)*R_2(y)$) with k=1 in the form

$$r(x,y) = C * (1 + \nu_1 e^{-(x-x_i)})^{-\frac{1}{\nu_1}} * (1 + \nu_2 e^{-(y-y_i)})^{-\frac{1}{\nu_2}} \quad (2)$$

where C is the fluorescent signal corresponding to the maximal concentration of AbAg complexes. Both terms can be normalized to their own inflection points

$$r_n(x,y) = C_n * (\frac{1+\nu_1}{1+\nu_1 e^{-(x-x_i)}})^{\frac{1}{\nu_1}} * (\frac{1+\nu_2}{1+\nu_2 e^{-(y-y_i)}})^{\frac{1}{\nu_2}} \quad (3)$$

with the visual advantage of moving x_i and y_i to the same horizontal line z=1 and with the theoretical advantage of introducing relative thermodynamic activity (see explanation later). In this form C_n corresponds to the fluorescent signal of AbAg complexes at the inflection point of the functions.

A logarithmic transformation converts the proportional variance pattern to a constant variance pattern and thus the conversion makes the transformed data more suitable for fitting the model. The above multiplicative relationship then changes to an additive one ($\ln R_1(x)+\ln R_2(y)$) in the form of

$$\ln r_n(x,y) = \ln(C_n) + \frac{1}{\nu_1}\ln(\frac{1+\nu_1}{1+\nu_1 e^{-(x-x_i)}}) + \frac{1}{\nu_2}\ln(\frac{1+\nu_2}{1+\nu_2 e^{-(y-y_i)}}) \quad (4)$$

This normalized, generalized logistic model on the log-log scale was fit to the data, and parameter estimates and 95% confidence intervals were obtained using the R software (version 3.5.2). Nonlinear least squares estimates for the model parameters were calculated using the Gauss-Newton algorithm of the *nls* function from the statistical software package R (version 3.5.2). Confidence intervals generated for the model parameters were based on the Wald-based technique. Figures are representative of 2 or 3 independent experiments.

3. Results

3.1 Definition of standard state of polyclonal antibody interactions

In chemical thermodynamics the standard state is a precisely defined reference state, which serves as a common reference point for the comparison of thermodynamic properties. The standard chemical potential is arbitrarily defined in any system in a way to suit the description of the system. For the purpose of chemical reactions pressure, temperature and material composition can define a standard state. Pressure and temperature do not usually change in a living organism and for an immunoassay we can use and define conditions identical to those *in vivo*: 1 bar and 37°C. The chemical potential of an antibody solution, besides the concentration of the antibody itself, depends primarily on the concentration of the target molecules, antigens. We have recently described the modeling of antibody binding to antigen microspots by the product of two Richards functions. Each of the Richards functions represents the growth of the relative concentration of bound reactants, one as a function of the logarithm of Ag density, the other as a function of the logarithm of Ab concentration (Figure 1A). The product of these functions can be visualized by a 3D surface plot (Figure 1B).

In this system the inflection points of the two functions can serve as the origin of coordinates. We therefore define the standard state of a particular serum antibody and particular antigen mixture via the definition of the standard concentrations of antibody and antigen required to reach the point of inflection along both titration axes. In general, it means that each serum antibody-antigen pair will have a distinct standard state and the identified standard state concentrations will therefore characterize the serum sample in terms of its reactivity against the tested Ag.

To obtain thermodynamic parameters relative to the so defined standard state we normalize the Richards function as

$$\frac{c_{b_x}}{c_{b_{x^\circ}}} \equiv R_n(x)/A_n = \left(\frac{1+\nu}{1+\nu e^{-k(x-x^\circ)}}\right)^{\frac{1}{\nu}} \qquad (5)$$

where c_b is the concentration of bound molecules at titration concentration x or at standard concentration x°, x is the concentration of the titrated molecule and $R_n(x)$ is the Richards function normalized so that the value of the function is 1 at the point of inflection, x°. Again, we assume k=1. In this parametrization ν is the asymmetry parameter in the Richards function and the exponent of the corresponding Richards differential equation (43).

The fitting is carried out with the logarithmic forms of the two functions as

$$\ln(FI) = \ln(C_n) + \ln\left\{\left(\frac{1+\nu_1}{1+\nu_1 e^{-k(\ln[Ag]-\ln[Ag]^\circ)}}\right)^{\frac{1}{\nu_1}}\right\} + \ln\left\{\left(\frac{1+\nu_2}{1+\nu_2 e^{-k(\ln[Ab]-\ln[Ab]^\circ)}}\right)^{\frac{1}{\nu_2}}\right\} \qquad (6)$$

where C_n stands for the fluorescence intensity of the standard complex concentration [AbAg]°. Curve fitting delivers the estimated values for C_n, ν_{Ag}, ν_{Ab}, ln[Ag]° and ln[Ab]°.

The concentration of AbAg complexes is a cumulative measure of the activity of both components: by increasing the concentration of either, more and more complexes are formed. Activity, on the other hand, is the rate of change of complex formation, which is given by the partial derivatives of the fitted surface. We propose therefore, that once the above parameters of the functions are estimated, the relative thermodynamic activity of the complex at various Ab and Ag concentrations can be obtained from the products of the derivatives of Richards functions R_1'(ln[Ag])*R_2'(ln[Ab]) as shown in Figure 1C.

Figure 1.

The thermodynamic activity coefficient γ_{Ag} adjusts concentration to activity by accounting for non-ideality in the reaction. In our experimental system non-ideality is the complex nature of binding of a heterogenous mixture of antibodies with different affinities and concentrations and their interactions. The activity coefficient γ_{Ag} therefore changes as the concentration and interactions of antibodies change as a function of Ag density. By increasing [Ag], as the number of antibody molecules accessible for binding gradually decreases, the binding curve approaches an upper limit. This is associated with decreasing activity coefficient.

So far we assumed that activity is given by R'(x) and relative concentration by R(x). Now we consider the thermodynamic relationship

$$a = \gamma * c/c^{\circ} \quad (7)$$

where a is relative thermodynamic activity, γ is activity coefficient and c/c° is relative concentration. Comparing that to the general mathematical relationship between cumulative, absolute and relative growth functions (47), which corresponds to the mathematical identity

$$R'(x) = (\ln R)'(x) * R(x) \quad (8)$$

where R' is the derivative of, (lnR)' is derivative of the logarithm of, and R is the Richards function,

we deduce that the activity coefficient is given by the derivative of the logarithm of R, (lnR)'(x). Thus, in our model all these thermodynamic variables can be calculated by various transformations of the Richards function.

While γ adjusts concentration for non-ideality of reaction conditions, the limiting activity coefficient γ^{∞}, also called activity coefficient at infinite dilution, describes the limits of such non-ideality. For solutions this means that at infinite dilution solute molecules are completely surrounded by solvent molecules and only solvent-solute interactions determine the value of the coefficient. In a similar manner at infinite Ag dilution Ag molecules are completely surrounded by Ab molecules, and the value of the limiting activity coefficient γ_{Ag}^{∞} characterizes the binding properties of serum antibodies. Thus, for a given system of serum and Ag the value of γ^{∞} is constant, unlike γ, which changes with the composition of the system. In our description of the system using normalized functions, the limiting activity coefficients are related to the asymmetry parameter of the Richards function and are given by

$$\gamma_x^{\infty} = \frac{1+\nu}{\nu} \quad (9)$$

(see online **extended data** for derivation). Overall, in our model the equilibrium concentration of [AbAg] for each [Ab] and [Ag] composition is obtained by the estimation of the standard state concentrations [Ab]°, [Ag]° and the limiting coefficients γ_{Ag}^{∞} and γ_{Ab}^{∞} .

3.2 Assessment of measurement performance

Each subarray of the microarray slide contained a dilution series of a mixture of purified human IgM, IgG and IgA, which we used as reference measurement points for calibration. Two antigen microarray slides were treated identically with serum, then one developed for heavy-chain specific, the other for light chain specific antibodies. Calibration curves obtained after excluding variable weak signals and fitting linear regression curves to log-log datasets are shown in Figure 2A. The intra-assay and interassay variability of fluorescent detection and the linearity of ln(signal)-ln([Ab]) relationship was calculated from these data. Based on these results, fluorescence signals below 40 FI were excluded from further analysis. The calibration curves obtained were used for calculating absolute serum Ab concentrations and chemical potential, discussed under section 3.4.

Figure 2.

We used the monoclonal antibody AD1.1.10, specific for the hexahistidine tag engineered to the C-terminus of the recombinant RBD, to examine the performance of the measurement system and the fitting strategy with an antibody of known concentration. A series of different dilutions of the antibody was reacted with the microarray and detected using a goat anti-mouse IgG antibody with Alexa-488 label. The data was then fitted using the above algorithm and key thermodynamic parameters calculated (Figure 2B). Curves fitted to the measurement points with the combination of lnR functions are shown for varying Ag and Ab concentrations (upper panels). Individual lnR functions give the relative concentrations of bound components (bottom panels). The obtained [Ag]° and [Ab]° values were different by orders of magnitude, underlining the distinct behavior of soluble Ab and surface immobilized Ag molecules in the measurement system. The calibration results indicated that the measurement system can be applied to estimate Ab concentrations from low nanomolar to micromolar range, while fitting precision decreases as signals approach background noise.

3.3 Estimation of primary thermodynamic variables of SARS-CoV-2 specific serum Ab

Following the introduction of SARS-CoV-2 vaccines in early 2021, we collected blood samples from people working in the laboratory to confirm seroconversion and monitor effects of repeated shots. In this paper we present results obtained from 4 individuals at two different timepoints (Table 1).

Table 1.

We designed the microspot assay so as to be able to obtain several measurement points possibly even for weakly reactive samples, by using dense Ag microspots and minimally diluted serum, but a sample deemed seronegative with conventional commercial assay could not be fitted for the binding of any immunoglobulin class. Other samples were fitted with varying efficiency, with kappa light chain and IgG detection providing the most abundant and best fittable signals.

In the representation of logarithmic normalized Richards functions the value of ln[Ag] at $\ln R_n=0$ identifies the inflection point ln[Ag]° of the function and thus the standard state concentrations (Figure 3A). The distance from this intersection for serum dilutions is the relative concentration (Figure 3B). The value of γ^{∞} influences the slope of the left asymptote and the position of the upper asymptote: a higher γ^{∞} results in a steeper curve (slope of left asymptote) and greater upper asymptote. That translates as a faster fall in reactivity with concentrations decreasing below the standard state, and a higher concentration of bound component relative to the standard state with concentration increasing above the standard state. On the molecular level this means that binding is dominated by low affinity interactions, which become undetectable quickly below standard concentration, but result in significant binding above the standard concentration. SARS-CoV-2 RBD binding curves of serum samples obtained by titrating Ag and Ab were generated from the results of fitting are shown in Figure 4.

Figure 3.

Figure 4.

A smaller value of ln[Ag]° signifies that the binding curve of detected antibody class reaches an inflection point at lower Ag concentration, which can be interpreted as higher average affinity. Binding curves in general showed higher variability when [Ab] rather than [Ag] was varied, indicating that immune response variability is dominated by differences in concentration rather than affinity in the examined samples. When measurable (four samples), IgA affinity was distinctly lower within two samples (samples G-G-14 and G-G-16) than other isotypes.

3.4 Calculation of specific serum Ab concentrations and partial chemical potential

While the relative Ab concentration is an ideal parameter for characterizing the ability of an Ab to occupy Ag binding sites, using the calibration curve we can also calculate absolute concentrations. This not only allows us to estimate specific serum Ab concentrations but also to calculate [Ab]° and, assuming a 1:1 stoichiometry, the standard concentration of the complex [AbAg]°.

Chemical potential is expressed as

$$\mu = \mu^\circ + RT\ln a \qquad (10)$$

where μ is chemical potential, μ° is standard chemical potential, R is universal gas constant, T is thermodynamic temperature, and *a* is relative thermodynamic activity. The chemical potential indicates the ability of a substance to contribute particles to a physical system. As the above equation shows, under standard conditions it equals the standard chemical potential. In our case it is determined by the rate of change of concentration [AbAg] in the standard state and is proportional to the sum of the logarithm of standard complex concentration and the logarithm of thermodynamic activity.

$$\mu = RT\ln[AbAg]^\circ + RT\ln a = RT(\ln[AbAg]^\circ + \ln a) \qquad (11)$$

$$\mu/RT = \ln[AbAg]^\circ + \ln a \qquad (12)$$

The first term can be calculated using the calibration curve and the second term is obtained by taking the logarithm of the derivative of Richards function, lnR' (Figure 5). By our definition, chemical potential is highest in the standard state, corresponding to the peak in Figure 4. Relative thermodynamic activity *a* decreases on both sides, corresponding to decreasing chemical potential either by decreasing or by increasing the availability of Ag, expressed as ln[Ag]. On the other hand, the coordinates of the peak identify the relationship between [Ag]° and [AbAg]°. Asymmetry in the curve depicting chemical potential of the complex in the presence of varying concentrations of Ag is governed by the limiting activity coefficient. Higher values of γ_{Ag}^{∞} are indicative of a faster fall of potential with decreasing ln[Ag].

Fig.5.

We used the calibration curves shown in Figure 2A to calculate [AbAg]° concentrations for all five measured immunoglobulin isotypes. Figure 6 shows the relationships between relative serum Ab concentrations (A) and standard AbAg concentrations (B) against the standard Ag concentrations for each isotype. The ranks of individual serum samples are different for these variables, indicating that they capture different aspects of Ab reactivity: the first is a quantitative, while the second is a qualitative property. Figure 6C displays how the chemical potential of AbAg complexes changes in the presence of

different concentrations of Ag. Complexes have maximal potential (by definition) in the standard state (Figure 6B), decreasing both in the presence of limiting (left side of peak) and excess (right side of peak) Ag concentrations. The rate of decrease is determined by the limiting activity coefficient as modeled by the logarithm of the derivative of normalized Richards function $\ln(R_{1n}')$.

Figure 6.

3.5 Comparison of dual titration with a conventional serological method

All tested samples were analyzed with a commercial, routinely used, automated chemiluminescent immunoassay for SARS-CoV-2 spike specific Ab (S-Ig), which measures all serum antibodies that can bridge an immobilized Ag and a labeled Ag, in other words capable of bivalent binding. The relationship between dual titration results and the assay are presented in correlation plots in Figure 7.

Figure 7.

4. Discussion

Conventional approaches to the qualitative and quantitative characterization of specific serum antibodies yield arbitrary units or titers. In order to obtain biochemically meaningful, truly quantitative results, we applied physical chemistry in the interpretation of microspot antigen titration results. First, we defined the standard chemical thermodynamic state of a particular antigen molecule in a particular serum with respect to a particular antibody class that is measured. The aim of the measurement itself is then the estimation of antigen density in the microspot and the relative antibody concentration of serum antibodies required to bring the system to the standard state. If the measurement data are suitable to identify the standard state, we can model the behavior of the system under different conditions.

By employing the combination of two Richards functions, for fitting both Ab and Ag titration curves, we obtain values of the key variables: standard state concentrations and limiting activity coefficients. A 3D surface plot of the relative thermodynamic activity of Ab-Ag complexes (Figure 1C) identifies Ab and Ag concentrations at which changes in either of them bring about the greatest change in free energy. On one hand that means the immune system is tuned to sensitively respond to changes in [Ag] in this range. On the other hand, it is this [Ab] that efficiently maintains [Ag] at this level. Changing [Ag] will trigger B-cell receptor signals in memory B cells, leading to expansion and Ab production (43). Thus, the standard state corresponds to maximal relative thermodynamic activity and represents a steady state the immune system ideally maintains towards this particular antigen. This state is a function of B-cell differentiation, which determines affinity (48), antigen abundance, which drives B-cell proliferation (49), and immune complex removal through Fc receptors, which maintains the flow of antigen towards molecular degradation (50).

Serological measurements play a key role during pandemics in several aspects: they allow seroepidemiological monitoring of disease spread, assessment of individual responses against pathogens or vaccines and as a correlate of protection from disease. Multitudes of various assays had been developed recently for SARS-CoV-2 serology, with different platforms, antigens, methods and aims. Neutralization assays are considered good correlates of protection and they show correlations with serological measurements. The determination of Ab affinity has also been suggested to provide useful clinical information (51,52). Unfortunately, most of these assays generate distinct results in terms of units and comparability even after transformations. An assay with truly quantitative readout of chemical

properties of SARS-CoV-2 specific antibodies could substantially improve our immunological understanding of COVID serology. Our observations on this limited set of serum samples already provide interesting insights. The immune system deploys various immunoglobulin classes and various combinations of Ab affinity and concentration increases in response to SARS-CoV-2 vaccinations. Profiles of kappa light chain detection were similar to IgG detection, indicating that specific antibodies carrying kappa light chain dominantly belong to the IgG class. This is corroborated by the fact that specific serum IgG concentrations were the highest (Fig 4.A). It is important to note the crossing of curves in Figure 3: it indicates that owing to the heterogeneity of Ab, which is captured by the variable γ^{∞}, the rank of binding efficiency of samples changes both with Ag density and serum dilution. This is the reason why single-point measurements, in the sense of single Ag density and single serum dilution, are unable to accurately characterize serum Ab reactivity. Titration of serum dilution makes a step towards a deeper analysis, but it requires dual titration to be able to deconvolve the effects of affinity and concentration.

A key novelty of our approach is the use of chemical potentials for the characterization of interactions between Ab and Ag. The biochemical term affinity has been used for the characterization of the strength of binding between a given Ag molecule and Ab molecules. This makes sense for a monoclonal antibody, where the equilibrium constant K is the ratio of [AbAg]/([Ab]*[Ag]) and is a measure of binding affinity. In this case a single binding site is considered and all three components have definite concentrations. In the blood serum millions of Ab binding sites are present, corresponding to the millions of distinct Ab structures produced in the host organism. Any Ag molecule that comes into contact with serum therefore probes those millions of binding sites, what we observe upon measuring bound Ab is the cumulative result of a distribution of binding strengths. We no longer speak of distinct concentrations and affinities but rather of the cumulative strength and concentration of all binders. The aim of a humoral Ab response is the adjustment of concentration for each epitope recognized by the immune system. Recognition in this sense is the difference from average binding strength between macromolecules. This is tuned by the system over a very wide range, resulting from silent recirculation and degradation through efficient removal to immediate expulsion from the body. The concentration the immune system aims to adjust for a given Ag appears as the standard concentration [Ag]° in our measurements. Were there just a single Ab to adjust this concentration via a single interaction site of the Ag, we could talk about affinity and concentration in the above-mentioned classical context. This would be indicated by a limiting coefficient value of 2 and a "simple" logistic function. Instead of this theoretical case, the immune system deploys several structurally and clonally related Ab, which together show an apparent standard concentration [Ab]°. Importantly, this value - unlike for the monoclonal case - can be higher than [Ag]° because the thermodynamic activities of all binding Ab contribute to adjusting [Ag]. The greater the number of these distinct binders, the greater can be the difference between the two quantities. The other way round, the immune system can deploy many low affinity binder Ab to decrease [Ag] instead of using one very high affinity binder. Figure 4 shows the individual variability of these values for different Ab classes. The immune system has best control over [Ag] around [Ag]° because the farther it gets from this point the chemical potential of Ab decreases along with that of AbAg.

The commercial, conventional technology used here for comparison employs a capture bridge assay, where oligovalent Ab in the sample bridges solid-phase Ag to labeled Ag in solution. Comparing the rank of samples according to this assay (Figure 7) and the rank by Ag or Ab titration (Figure 4A) suggests that the above a certain affinity (kappa, ln[Ag]°>-13.7) it is the concentration that determines measurement outcome (kappa rank at ln[Ab]~-6.5). This corresponds to the fact that conventional assays use a single Ag density and single Ab dilution for characterizing Ab reactivity. In other words, the two weakest binding samples (B-16, G-G-16) were lowest in the rank, the others were ranked according to their relative binding $\ln([Ab_b]/[Ab_b]_i)$ at a given serum dilution. This is supported by the relationship between S-Ig and $\ln([Ab_{serum}]/[Ab]°)$ in Figure 7.

We found sufficient IgA reactivity for fitting in samples collected within a few weeks following BNT162b2 and Gam-COVID-Vac vaccinations. This is in agreement with the observation that these vaccines, though variably, elicit serum IgA (53–55). Affinity, as represented by ln[Ag]°, was highly variable in the samples, perhaps related to the fast but diminishing nature of IgA responses as described in those studies. Specific IgM was also detectable early after vaccination but not after prolonged periods. The measured chemical potentials of both IgA and IgM were below that of IgG (Figure 4), underlining the dominance of IgG in Ag binding in the serum. In humans, kappa light chains (incorporated into immunoglobulins, not as free chains) are usually about twice as frequent as lambda light chains both on B cells (56) and in serum immunoglobulins (57). We used kappa and lambda immunoglobulin detection as a means to measure a mixture of Ab with different heavy chains. The fitting efficiency and the pattern of reactivity of kappa chains was comparable to that of IgG, again suggesting the dominance of IgG immunoglobulins that use kappa chains.

Concentration expressed as the ratio of serum [Ab] to standard [Ab] is an effective concentration in the sense it is a measure of relative antigen occupancy: the binding rate changes most rapidly at the standard state (inflexion point) so the "distance" from this point, either above or below, is a good indicator of binding efficiency. We can also derive absolute concentration from this value and from [AbAg]° with the help of a standard curve for Ab (Figures 2 and 4). However, this number is also a function of the number of epitopes on the Ag and is therefore less suitable for comparing different Ag. Absolute specific antibody concentrations, rather than a measure of affinity, standard Ag concentration, seem to be related to the result of a conventional assay (Figure 7).

The relationship between circulating blood B cells can be characterized by the sequence similarity of their antibody coding genes (58,59). By single-cell sequencing the correct pairs of heavy and light chain immunoglobulin variable sequences can be obtained and used as an ID for each B cell. Ranks of similarity can then be used to generate clonal networks and trace B-cell differentiation during an immune response. In these networks, nodes represent cells, or more appropriately unique sequence pairs of antibody chains, and links represent similarity, corresponding to shared Ag binding properties. We recently proposed that hierarchy can be introduced into these networks by assuming that B-cell differentiation via somatic hypermutation results in antibodies with higher affinity to antigen (60). In the RADARS model higher affinity corresponds to a higher network degree, because links correspond to Ag transfer from lower to higher affinity Ab and high affinity Ab collect Ag from more lower affinity Ab. Similar sequences should show similar binding properties, thus sequence similarity corresponds to ability to transfer Ag between similar sequences. As the Ag seeks its binding partner with highest affinity it follows pathways of network links, from low to high affinity, towards higher degree nodes. The degree distribution of this network therefore corresponds to the probability density of antibodies with increasing thermodynamic activity. The degree distribution of a subnetwork, comprising only antibodies binding to a selected antigen molecule, in a similar manner, represents the probability density of antibodies binding to the selected antigen with increasing activity. For a scale free network with power law degree distribution, the exponent defines network properties. We propose that the limiting activity coefficient of Ag, γ_{Ag}^{∞} corresponds to the network degree distribution exponent of the antibody network contributing to the measurement, being an indicator of Ab composition (Figure 8).

Figure 8.

The current limitation of the method with respect to analytical sensitivity is the requirement of a sufficient number of datapoints from the measurement for curve fitting. For weakly reactive serum samples this is a difficult task as it would require a high number of very dense Ag microspots. As long as the characterization of sera that are positive for the given antigen is the goal it may not be a serious

shortcoming but it will be safer to work with a method that yields quantitative results even for negative samples. With respect to reproducibility, the accuracy of the Ag density in the microspots is critical. This property is determined and can be controlled during the production of microspot arrays, so it is not influenced by the development steps in the laboratory. Furthermore, absolute values of the signals are not affecting the results, which are derived from the properties of the curve instead. This study is not a systematic assessment of SARS-CoV-2 specific humoral immune response. We utilized blood samples collected for the purpose of confirming response to vaccinations, therefore these samples reflect responses at different stages of immunization and to different vaccine formulations but are not representative of either. The results show that SARS-CoV-2 specific immune responses can be subjected to a deep thermodynamic analysis using this technology if responses exceed a certain minimal threshold. Here we aimed to demonstrate the concept of application of physical chemistry to quantitative serology via the use of dual-titration and a normalized, generalized logistic function. Further studies using this approach will be needed to reveal the potency of the technology in discovering immunological phenomena not addressed by conventional technologies. We expect that technical improvements and larger scale production of the Ag microspot arrays will increase the efficiency of fitting and render the method suitable for routine use.

Overall, our technology is unique in the sense that it simultaneously estimates all relevant physico-chemical parameters relevant for immunochemical thermodynamic profiling of different Ab classes. The method is based on planar protein microarray technology, which is well-established and available by now in central laboratories. We envisage the application of this technology when a deeper analysis of serological reactivity is needed. In clinical diagnostics it could follow screening steps in the diagnostic algorithm. Once diagnosis is established, the truly quantitative data should be useful for monitoring and adjusting therapy. Beyond medical serology, the generation of antibody binding data with universal units should contribute to the generation of databases for systems immunology in general.

Data and Software Availability

Extended data

Mass spectrometry proteomics data of RBD protein.

PRIDe. LC-MS experiments of SARS-CoV2 Receptor Binding Domain WT. PXD040415.

Figshare: quantitative serology.

This project contains the following underlying data:

- Detailed microarray protocol. Detailed characterization of the design, generation and use of microspot immunoassay. https://doi.org/10.6084/m9.figshare.22202764
- Biochemical characterization of RBD protein. Description of the biochemical analysis of recombinant SARS-CoV-2 RBD protein quality. https://doi.org/10.6084/m9.figshare.22202809
- Derivation of the limiting thermodynamic activity coefficient. Description and mathermatical derivation of how the thermodynamic limiting activity coefficient is obtained from the asymmetry parameter of the Richards function. https://doi.org/10.6084/m9.figshare.22202803
- Different forms of the Richards function used for chemical thermodynamic analysis. A table containing the various transformations of the Richards function suitable for chemical thermodynamic analysis of antibody-antigen binding reactions. https://doi.org/10.6084/m9.figshare.22202833
- List of equations in the paper. Complete list of the mathematical formulae used in the paper. https://doi.org/10.6084/m9.figshare.22202827

- Data obtained and generated for quantitative serological measurements. A datasheet containing all the analyzed data after data cleaning (removal of outliers), fitting binding curves and calculating the derived variables. https://doi.org/10.6084/m9.figshare.22202863
- Raw data. Datasheet of all data used in the article directly from measurements, before fitting. https://doi.org/10.6084/m9.figshare.22240372

Author contributions

ÁK, TP and JP conceptualized the application of Richards curve to titration data. ÁK, ZH, KP curated the data obtained by measurements. KP and DNL carried out formal analysis of immunoassays and protein MS data, respectively. PS and JP arranged funding support. ZH and LB performed experiments. ZH, JZK, DNL and LB contributed to methods development. PS and JP administered the project. JZK, EU and JP provided resources for the project. ÁK worked out the fitting algorithm. EU, TP and JP supervised the project. KP and JP visualized concepts and data. ZH, JZK and JP prepared drafts; KP, TP and JP edited and finalized writing of the manuscript.

Grant information

No dedicated funding was used for this study.

Acknowledgments

JZK would like to thank Jonas Heilskov Graversen from the Institute of Molecular Medicine, University of Southern Denmark for the advice within plasmid design and construction.

Conflict of interest

K.P., Z.H. and J.P. are inventors in a patent submission by Diagnosticum Zrt, related to the technology described in this paper.

References

1. Cheng HD, Dowell KG, Bailey-Kellogg C, Goods BA, Love JC, Ferrari G, et al. Diverse antiviral IgG effector activities are predicted by unique biophysical antibody features. Retrovirology. 2021 Oct 30;18(1):35.

2. Chackerian B, Peabody DS. Factors That Govern the Induction of Long-Lived Antibody Responses. Viruses. 2020 Jan 7;12(1).

3. Choteau M, Scohy A, Messe S, Luyckx M, Dechamps M, Montiel V, et al. Development of SARS-CoV2 humoral response including neutralizing antibodies is not sufficient to protect patients against fatal infection. Sci Rep. 2022 Feb 8;12(1):2077.

4. Johnson M, Wagstaffe HR, Gilmour KC, Mai AL, Lewis J, Hunt A, et al. Evaluation of a novel multiplexed assay for determining IgG levels and functional activity to SARS-CoV-2. J Clin Virol. 2020 Aug 2;130:104572.

5. Farnsworth CW, Case JB, Hock K, Chen RE, O'Halloran JA, Presti R, et al. Assessment of serological assays for identifying high titer convalescent plasma. medRxiv. 2021 Mar 28;

6. Becker M, Strengert M, Junker D, Kaiser PD, Kerrinnes T, Traenkle B, et al. Exploring beyond clinical routine SARS-CoV-2 serology using MultiCoV-Ab to evaluate endemic coronavirus cross-reactivity. Nat Commun. 2021 Feb 19;12(1):1152.

7. Klasse PJ. Neutralization of virus infectivity by antibodies: old problems in new perspectives. Advances in Biology. 2014 Sep 9;2014.

8. Oguntuyo KY, Stevens CS, Hung CT, Ikegame S, Acklin JA, Kowdle SS, et al. Quantifying Absolute Neutralization Titers against SARS-CoV-2 by a Standardized Virus Neutralization Assay Allows for Cross-Cohort Comparisons of COVID-19 Sera. MBio. 2021 Feb 16;12(1).

9. Khoury DS, Cromer D, Reynaldi A, Schlub TE, Wheatley AK, Juno JA, et al. Neutralizing antibody levels are highly predictive of immune protection from symptomatic SARS-CoV-2 infection. Nat Med. 2021 Jul;27(7):1205–11.

10. Solastie A, Virta C, Haveri A, Ekström N, Kantele A, Miettinen S, et al. A Highly Sensitive and Specific SARS-CoV-2 Spike- and Nucleoprotein-Based Fluorescent Multiplex Immunoassay (FMIA) to Measure IgG, IgA, and IgM Class Antibodies. Microbiol Spectr. 2021 Nov 17;e0113121.

11. Murrell I, Forde D, Zelek W, Tyson L, Chichester L, Palmer N, et al. Temporal development and neutralising potential of antibodies against SARS-CoV-2 in hospitalised COVID-19 patients: An observational cohort study. PLoS ONE. 2021 Jan 26;16(1):e0245382.

12. Kubota K, Kitagawa Y, Matsuoka M, Imai K, Orihara Y, Kawamura R, et al. Clinical evaluation of the antibody response in patients with COVID-19 using automated high-throughput immunoassays. Diagn Microbiol Infect Dis. 2021 Mar 13;100(3):115370.

13. Garritsen A, Scholzen A, van den Nieuwenhof DWA, Smits APF, Datema ES, van Galen LS, et al. Two-tiered SARS-CoV-2 seroconversion screening in the Netherlands and stability of nucleocapsid, spike protein domain 1 and neutralizing antibodies. Infect Dis (Lond). 2021 Mar 8;1–15.

14. Cacaci M, Menchinelli G, Ricci R, De Maio F, Mariotti M, Torelli R, et al. Re-evaluating positive serum samples for SARS-CoV-2 specific IgA and IgG antibodies using an in-house serological assay. Clin Microbiol Infect. 2020 Dec 19;

15. Sette A, Crotty S. Adaptive immunity to SARS-CoV-2 and COVID-19. Cell. 2021 Feb 18;184(4):861–80.

16. Gaebler C, Wang Z, Lorenzi JCC, Muecksch F, Finkin S, Tokuyama M, et al. Evolution of Antibody Immunity to SARS-CoV-2. BioRxiv. 2021 Jan 4;

17. Qiu M, Shi Y, Guo Z, Chen Z, He R, Chen R, et al. Antibody responses to individual proteins of SARS coronavirus and their neutralization activities. Microbes Infect. 2005 May;7(5–6):882–9.

18. Heffron AS, McIlwain SJ, Amjadi MF, Baker DA, Khullar S, Sethi AK, et al. The landscape of antibody binding to SARS-CoV-2. BioRxiv. 2020 Oct 11;

19. Aydillo T, Rombauts A, Stadlbauer D, Aslam S, Abelenda-Alonso G, Escalera A, et al. Immunological imprinting of the antibody response in COVID-19 patients. Nat Commun. 2021 Jun 18;12(1):3781.

20. Rydyznski Moderbacher C, Ramirez SI, Dan JM, Grifoni A, Hastie KM, Weiskopf D, et al. Antigen-Specific Adaptive Immunity to SARS-CoV-2 in Acute COVID-19 and Associations with Age and Disease Severity. Cell. 2020 Nov 12;183(4):996-1012.e19.

21. Bölke E, Matuschek C, Fischer JC. Loss of Anti-SARS-CoV-2 Antibodies in Mild Covid-19. N Engl J Med. 2020 Oct 22;383(17):1694–5.

22. Hoepel W, Chen HJ, Geyer CE, Allahverdiyeva S, Manz XD, de Taeye SW, et al. High titers and low fucosylation of early human anti-SARS-CoV-2 IgG promote inflammation by alveolar macrophages. Sci Transl Med. 2021 Jun 2;13(596).

23. Selva KJ, van de Sandt CE, Lemke MM, Lee CY, Shoffner SK, Chua BY, et al. Systems serology detects functionally distinct coronavirus antibody features in children and elderly. Nat Commun. 2021 Apr 1;12(1):2037.

24. Atyeo C, Fischinger S, Zohar T, Slein MD, Burke J, Loos C, et al. Distinct Early Serological Signatures Track with SARS-CoV-2 Survival. Immunity. 2020 Sep 15;53(3):524-532.e4.

25. Dan JM, Mateus J, Kato Y, Hastie KM, Yu ED, Faliti CE, et al. Immunological memory to SARS-CoV-2 assessed for up to 8 months after infection. Science. 2021 Feb 5;371(6529).

26. Wajnberg A, Amanat F, Firpo A, Altman DR, Bailey MJ, Mansour M, et al. Robust neutralizing antibodies to SARS-CoV-2 infection persist for months. Science. 2020 Dec 4;370(6521):1227–30.

27. Nam M, Seo JD, Moon H-W, Kim H, Hur M, Yun Y-M. Evaluation of Humoral Immune Response after SARS-CoV-2 Vaccination Using Two Binding Antibody Assays and a Neutralizing Antibody Assay. Microbiol Spectr. 2021 Nov 24;e0120221.

28. Struck F, Schreiner P, Staschik E, Wochinz-Richter K, Schulz S, Soutschek E, et al. Vaccination versus infection with SARS-CoV-2: Establishment of a high avidity IgG response versus incomplete avidity maturation. J Med Virol. 2021 Dec;93(12):6765–77.

29. Chen Y, Yin S, Tong X, Tao Y, Ni J, Pan J, et al. Dynamic SARS-CoV-2-specific B-cell and T-cell responses following immunization with an inactivated COVID-19 vaccine. Clin Microbiol Infect. 2022 Mar;28(3):410–8.

30. Wu K, Werner AP, Koch M, Choi A, Narayanan E, Stewart-Jones GBE, et al. Serum Neutralizing Activity Elicited by mRNA-1273 Vaccine - Preliminary Report. N Engl J Med. 2021 Feb 17;

31. Pegu A, O'Connell S, Schmidt SD, O'Dell S, Talana CA, Lai L, et al. Durability of mRNA-1273 vaccine–induced antibodies against SARS-CoV-2 variants. Science. 2021 Aug 12;

32. Ebanks D, Faustini S, Shields A, Parry H, Moss P, Plant T, et al. Cross reactivity of serological response to SARS-CoV-2 vaccination with viral variants of concern detected by lateral flow immunoassays. J Infect. 2021 Jul 26;

33. Kritikos A, Gabellon S, Pagani J-L, Monti M, Bochud P-Y, Manuel O, et al. Anti-SARS-CoV-2 Titers Predict the Severity of COVID-19. Viruses. 2022 May 18;14(5).

34. Muecksch F, Wise H, Templeton K, Batchelor B, Squires M, McCance K, et al. Longitudinal variation in SARS-CoV-2 antibody levels and emergence of viral variants: implications for the ability of serological assays to predict immunity. medRxiv. 2021 Jul 7;

35. Bauer G. The potential significance of high avidity immunoglobulin G (IgG) for protective immunity towards SARS-CoV-2. Int J Infect Dis. 2021 May;106:61–4.

36. Prechl J. Why current quantitative serology is not quantitative and how systems immunology could provide solutions. Biologia Futura. 2021 Feb 20;

37. Busch NA, Chiew YC, Yarmush ML, Wertheim MS. Development and validation of a simple antigen–antibody model. AIChE J. 1995 Apr;41(4):974–84.

38. Lippok S, Seidel SAI, Duhr S, Uhland K, Holthoff H-P, Jenne D, et al. Direct detection of antibody concentration and affinity in human serum using microscale thermophoresis. Anal Chem. 2012 Apr 17;84(8):3523–30.

39. Berzofsky JA. The assessment of antibody affinity from radioimmunoassay. Clin Chem. 1978 Mar;24(3):419–21.

40. Nisonoff A, Pressman D. Heterogeneity and average combining constants of antibodies from individual rabbits. J Immunol. 1958 Jun;80(6):417–28.

41. Paul WE. Fundamental Immunology. 5th ed. Philadelphia: Lippincott Williams & Wilkins; 2003.

42. Papp K, Kovács Á, Orosz A, Hérincs Z, Randek J, Liliom K, et al. Absolute Quantitation of Serum Antibody Reactivity Using the Richards Growth Model for Antigen Microspot Titration. Sensors. 2022 Jan;

43. Prechl J, Papp K, Kovács Á, Pfeil T. The binding landscape of serum antibodies: how physical and mathematical concepts can advance systems immunology. Antibodies (Basel). 2022 Jun 23;11(3):43.

44. Rappsilber J, Mann M, Ishihama Y. Protocol for micro-purification, enrichment, pre-fractionation and storage of peptides for proteomics using StageTips. Nat Protoc. 2007;2(8):1896–906.

45. Perez-Riverol Y, Bai J, Bandla C, García-Seisdedos D, Hewapathirana S, Kamatchinathan S, et al. The PRIDE database resources in 2022: a hub for mass spectrometry-based proteomics evidences. Nucleic Acids Res. 2022 Jan 7;50(D1):D543–52.

46. Pfeil T, Herbály B. A linear model for polyclonal antibody–antigen reactions. Math Comput Simul. 2022 Aug;198:20–30.

47. Pommerening A, Muszta A. Relative plant growth revisited: Towards a mathematical standardisation of separate approaches. Ecol Modell. 2016 Jan;320:383–92.

48. Prechl J. A generalized quantitative antibody homeostasis model: regulation of B-cell development by BCR saturation and novel insights into bone marrow function. Clin Transl Immunology. 2017 Feb 17;6(2):e130.

49. Prechl J. A generalized quantitative antibody homeostasis model: antigen saturation, natural antibodies and a quantitative antibody network. Clin Transl Immunology. 2017 Feb 24;6(2):e131.

50. Prechl J. A generalized quantitative antibody homeostasis model: maintenance of global antibody equilibrium by effector functions. Clin Transl Immunology. 2017 Nov 17;6(11):e161.

51. Bauer G, Struck F, Staschik E, Maile J, Wochinz-Richter K, Motz M, et al. Differential avidity determination of IgG directed towards the receptor-binding domain (RBD) of SARS-CoV-2 wild-type and its variants in one assay: Rational tool for the assessment of protective immunity. J Med Virol. 2022 Jul 18;

52. Fiedler S, Piziorska MA, Denninger V, Morgunov AS, Ilsley A, Malik AY, et al. Antibody Affinity Governs the Inhibition of SARS-CoV-2 Spike/ACE2 Binding in Patient Serum. ACS Infect Dis. 2021 Aug 13;7(8):2362–9.

53. Takamatsu Y, Omata K, Shimizu Y, Kinoshita-Iwamoto N, Terada M, Suzuki T, et al. SARS-CoV-2-Neutralizing Humoral IgA Response Occurs Earlier but Is Modest and Diminishes Faster than IgG Response. Microbiol Spectr. 2022 Oct 11;e0271622.

54. Adjobimey T, Meyer J, Sollberg L, Bawolt M, Berens C, Kovačević P, et al. Comparison of IgA, IgG, and Neutralizing Antibody Responses Following Immunization With Moderna, BioNTech, AstraZeneca, Sputnik-V, Johnson and Johnson, and Sinopharm's COVID-19 Vaccines. Front Immunol. 2022 Jun 21;13:917905.

55. Sheikh-Mohamed S, Isho B, Chao GYC, Zuo M, Cohen C, Lustig Y, et al. Systemic and mucosal IgA responses are variably induced in response to SARS-CoV-2 mRNA vaccination and are associated with protection against subsequent infection. Mucosal Immunol. 2022 May;15(5):799–808.

56. Levy R, Warnke R, Dorfman RF, Haimovich J. The monoclonality of human B-cell lymphomas. J Exp Med. 1977 Apr 1;145(4):1014–28.

57. Normansell DE. Use of kappa and lambda chain quantitation for the detection of immunoglobulin abnormalities in serum. Diagn Clin Immunol. 1987;5(2):100–3.

58. Devulapally PR, Bürger J, Mielke T, Konthur Z, Lehrach H, Yaspo M-L, et al. Simple paired heavy- and light-chain antibody repertoire sequencing using endoplasmic reticulum microsomes. Genome Med. 2018 Apr 27;10(1):34.

59. Friedensohn S, Lindner JM, Cornacchione V, Iazeolla M, Miho E, Zingg A, et al. Synthetic standards combined with error and bias correction improve the accuracy and quantitative resolution of antibody repertoire sequencing in human naïve and memory B cells. Front Immunol. 2018 Jun 20;9:1401.

60. Prechl J. Network organization of antibody interactions in sequence and structure space: the RADARS model. Antibodies (Basel). 2020 May 6;9(2).

Legends to figures

Figure 1. Calculation of standard state of AbAg complexes.

A) A measurement matrix is created from the dual titration, using the logarithm of Ab and Ag concentrations (ln[Ab], ln[Ag]) and of the detected fluorescent intensity signals (ln(FI)). B) The combination of lnR functions (lnR1+lnR2) is used for fitting binding data, which corresponds to obtaining the parameters of an AbAg binding surface in three dimensions. C) An activity plot obtained from the product of the derivatives of two Richards functions (R1'*R2'), reveals the standard state as the conditions with highest relative thermodynamic activity (a).

Figure 2. Calibration of Ab binding signals and curve fitting.

A) A mixture of purified immunoglobulins was used to relate fluorescent signals of binding (FI) to molar concentration, using linear regression (blue lines, equations and R square values are shown). Averaged signals of printed Ig mix from all subarrays of an individual slide are represented by each line. B) A monoclonal antibody specific for the hexahistidine tag in the recombinant viral RBD was used to characterize the fitting algorithm. The upper panels show measurement data (symbols) and fitted curves for each titration curve. The lower panels show the curves of normalized R_1 and R_2 functions, for Ag and Ab titration, respectively. Confidence intervals are represented by dashed lines.

Figure 3. Interpretation of fitted binding curves.

The binding curves obtained by titration of A) Ag and B) Ab are shown. A) The logarithm of normalized R1 function intersects the horizontal axis at the logarithm of standard Ag concentration. B) The distance of the intersection of logarithm of normalized R2 function from the origo (red double arrow) is the logarithm of Ab concentration relative to standard Ab concentration. The slope of the left asymptote is determined by the respective limiting activity coefficients. [Ag], concentration of printed Ag; [Ab], 1/serum dilution factor; [Agb], concentration of Ag bound to Ab; $[Agb]_i$, concentration of Ag bound to Ab when ln[Ag]=ln[Ag]°; [Abb], concentration of Ab bound to Ag; [Abb]i, concentration of Ab bound to Ag when ln[Ab]=ln[Ab]°; γ_Ag^∞, limiting activity coefficient of Ag; slope of asymptote s is γ_Ag^∞/(1+v)/k; γ_Ab^∞, limiting activity coefficient of Ab; slope of asymptote s' is γ_Ab^∞/(1+v')/k.

Figure 4. Estimation of primary thermodynamic variables of antibody activity.

The Richards function R gives an estimate of the ratio (y axis) of the concentration of bound component at given total component concentration (x axis) over the concentration of bound component at the inflection point of the curve. Using the normalized R function, the curves intersect with 0 value of lnR exactly at the standard concentration, making it easy to identify ln[Ag]° (R_1, left diagrams) and ln[Ab]° (R_2, right diagrams). This representation is suitable for the comparison of A) a given Ab isotype of distinct individuals or B) distinct Ab isotypes of individuals (use roll-down menus for selection).

Figure 5. Detailed quantitation of serum antibody properties.

A) The primary variables obtained for a serum sample by fitting binding data can be combined in a single plot. The red double arrow corresponds to the same in Figure 3. B) Absolute concentrations of serum antibodies can be calculated from relative concentrations using calibration curve equations. C) The chemical potential of serum antibodies at different compositions can be calculated using the logarithm of the derivative of R1 function.

Figure 6. Primary and calibration-derived variables of Ab.

A) Combined visualization of primary variables, relative concentration [Abserum]/[Ab]° against ln[Ag]°, is suitable for mapping Ab activity of individuals and immunoglobulin isotypes (select isotype and sample for visualization). B) Using the immunoglobulin calibration curves, standard concentrations of AbAg complexes can be calculated, here displayed as logarithm of concentration (ln[AbAg]°) against logarithm of standard Ag concentration (ln[Ag]°). C) The change of AbAg chemical potentials as a function of logarithm of Ag concentration (ln[Ag]) is governed by the limiting activity coefficient, with μ peaking at the standard AbAg concentration.

Figure 7. Correlation plots of dual titration variables and conventional serology.

Values of A) logarithm of standard Ag concentration (ln[Ag]°) and B) logarithm of relative Ab concentration ln ([Abserum]/[Ab]°) are displayed against results of an automated serological test (S-Ig).

Figure 8. Molecular interpretation of the variables.

Clones of antibodies with different fine specificities and affinities bind to epitopes of the antigen used in the assay. Titration and curve fitting characterizes the distribution of binding activity and provides both an average affinity and an index of clonal composition.

individual ID	sample ID	vaccination status (vaccine, post-vaccination days)	serology S-Ig (BAU)	successful fitting
#1	#1-1	B-16	48.8	GMkl
	#1-2	B-B-B-12	31560.0	GMAkl
#2	#2-1	G-G-16	44.0	GMAkl
	#2-2	G-G-134	207.0	kl
#3	#3-1	G-G-14	1231.5	GMAkl
	#3-2	G-G-180	234.5	Gk
#4	#4-1	H-H-18	0.7	-
	#4-2	H-H-B-22	11925.0	GMAkl
	#4-3	H-H-B-36	9450.0	Gk

Table 1. Serum samples and fitting efficiency.

Vaccination status indicates the type of vaccine received and the days past last vaccination. Conventional serology results for viral spike Ig are shown and the fitting success, indicating the heavy (G,M,A) and light (k,l) chain isotypes for which the Richards functions were successfully fitted. G, Gam-COVID-Vac(Sputnik V); B, BNT162b2(Pfizer-BioNTech); H, HB02(Sinopharm)

Figure 1.

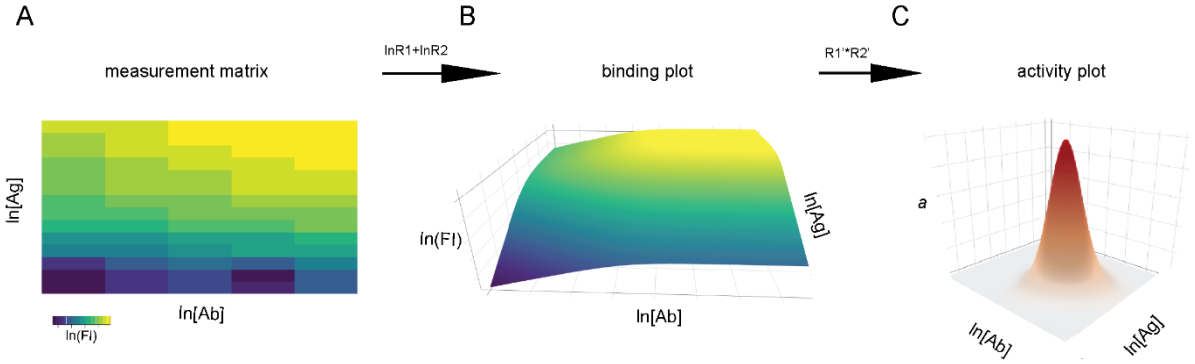
A
measurement matrix
ln[Ag]
ln[Ab]
ln(FI)
lnR1+lnR2
B
binding plot
ln(FI)
ln[Ag]
ln[Ab]
R1'*R2'
C
activity plot
a
ln[Ab]
ln[Ag]

Figure 2.

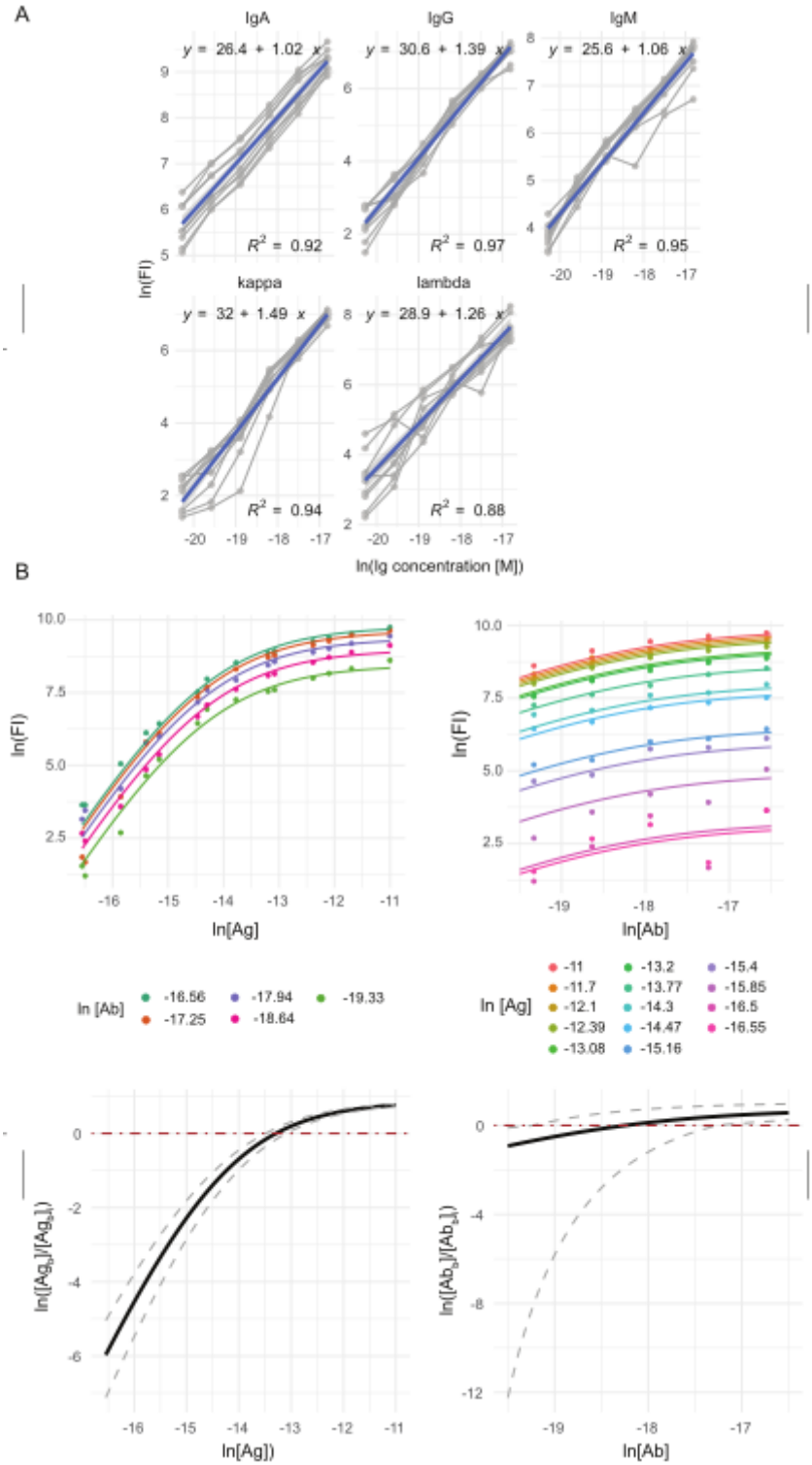
A
IgA
y = 26.4 + 1.02 x
R² = 0.92
IgG
y = 30.6 + 1.39 x
R² = 0.97
IgM
y = 25.6 + 1.06 x
R² = 0.95
kappa
y = 32 + 1.49 x
R² = 0.94
lambda
y = 28.9 + 1.26 x
R² = 0.88
ln(FI)
ln(Ig concentration [M])
B
ln(FI)
ln[Ag]
ln [Ab]
-16.56
-17.25
-17.94
-18.64
-19.33
ln(FI)
ln[Ab]
ln [Ag]
-11
-11.7
-12.1
-12.39
-13.08
-13.2
-13.77
-14.3
-14.47
-15.16
-15.4
-15.85
-16.5
-16.55
ln([Ag_b]/[Ag_u])
ln[Ag])
ln([Ab_b]/[Ab_u])
ln[Ab]

Figure 3.

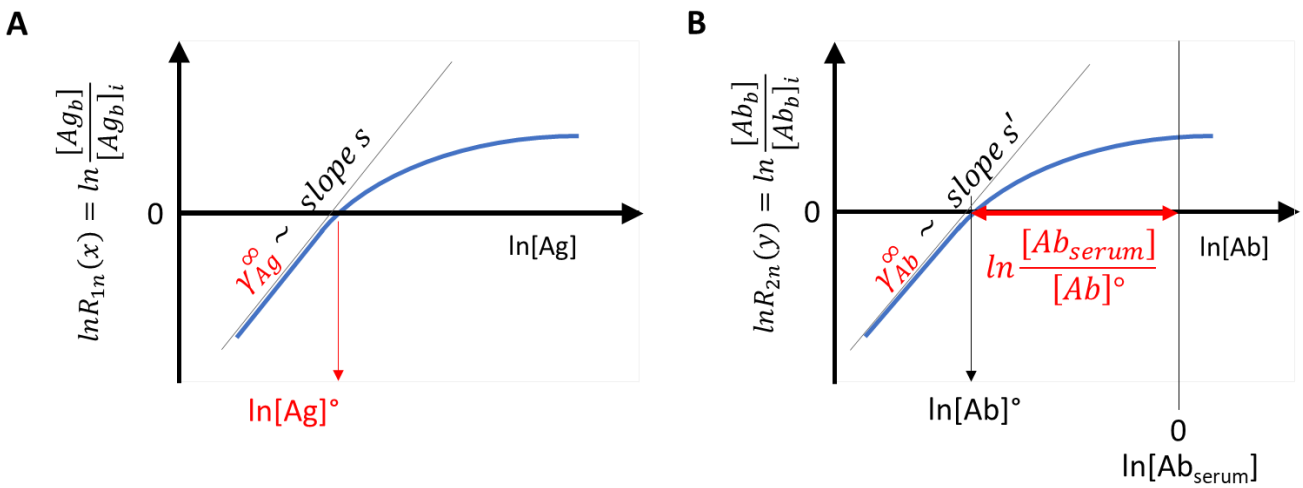
A
$lnR_{1n}(x) = ln\frac{[Ag_b]}{[Ag_b]_i}$
0
slope s
γ_{Ag}^{∞} ~
ln[Ag]
ln[Ag]°
B
$lnR_{2n}(y) = ln\frac{[Ab_b]}{[Ab_b]_i}$
0
slope s'
γ_{Ab}^{∞} ~
$ln\frac{[Ab_{serum}]}{[Ab]°}$
ln[Ab]
ln[Ab]°
0
ln[Ab$_{serum}$]

Figure 4. [screentshots of interactive Plotly diagrams]

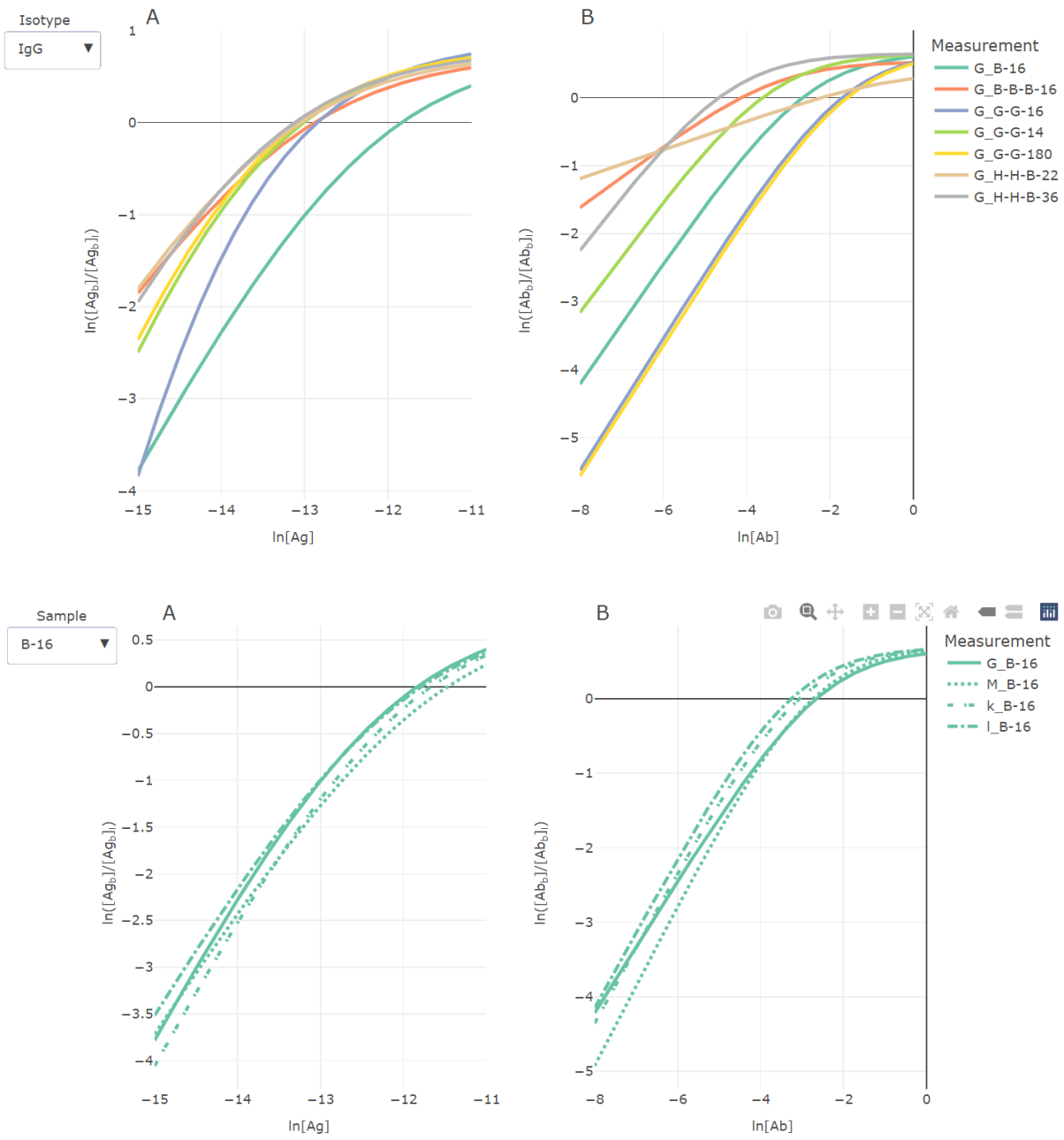

Figure 5.

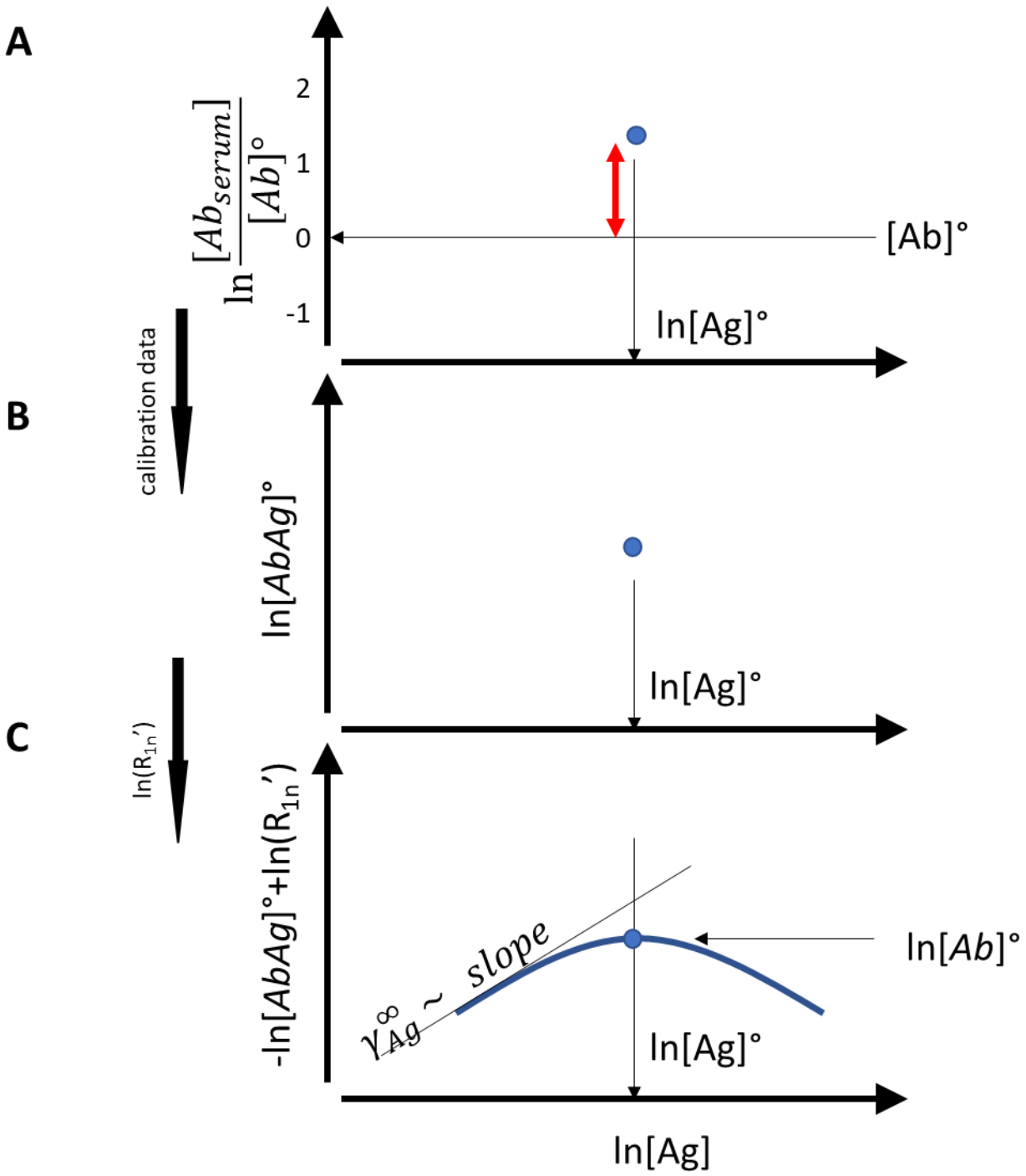
A
B
C
calibration data
ln(R1n')
2
1
0
-1
ln[Abserum]/[Ab]°
[Ab]°
ln[Ag]°
ln[AbAg]°
ln[Ag]°
-ln[AbAg]°+ln(R1n')
γAg∞ ~ slope
ln[Ab]°
ln[Ag]°
ln[Ag]

Figure 6. [screenshot from interactive Plotly diagram]

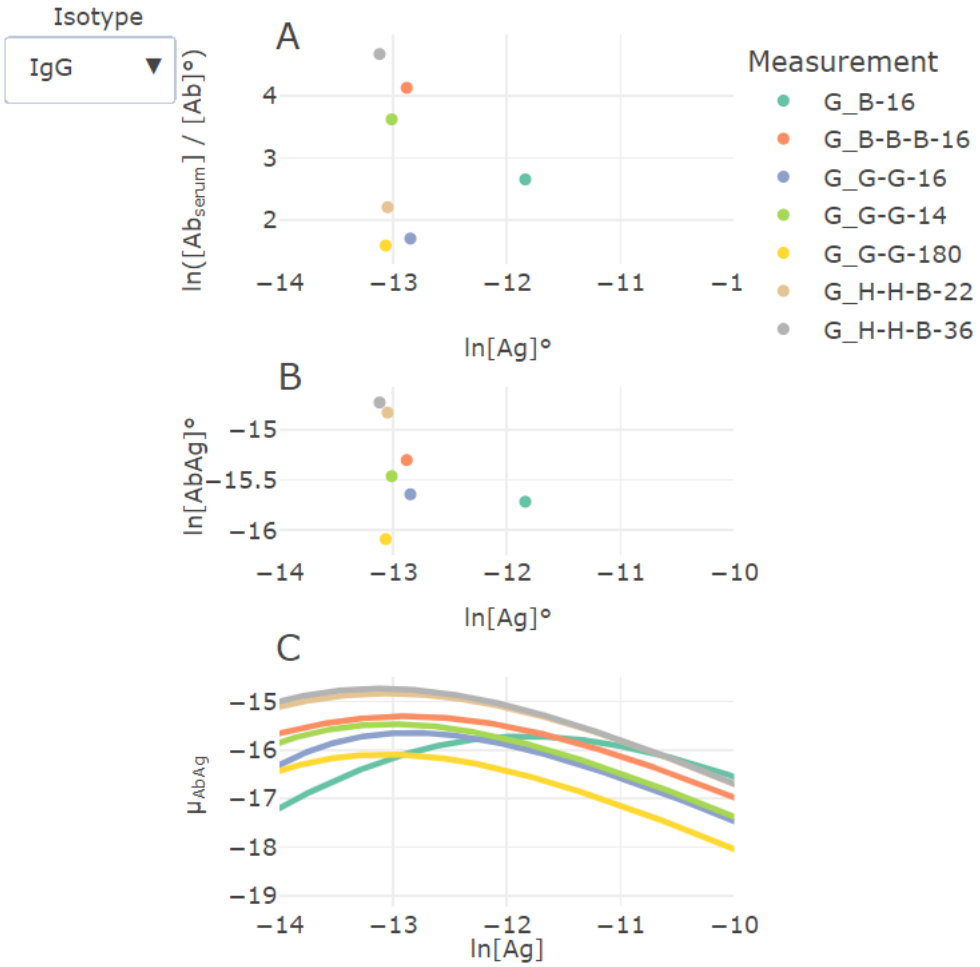

Figure 7.

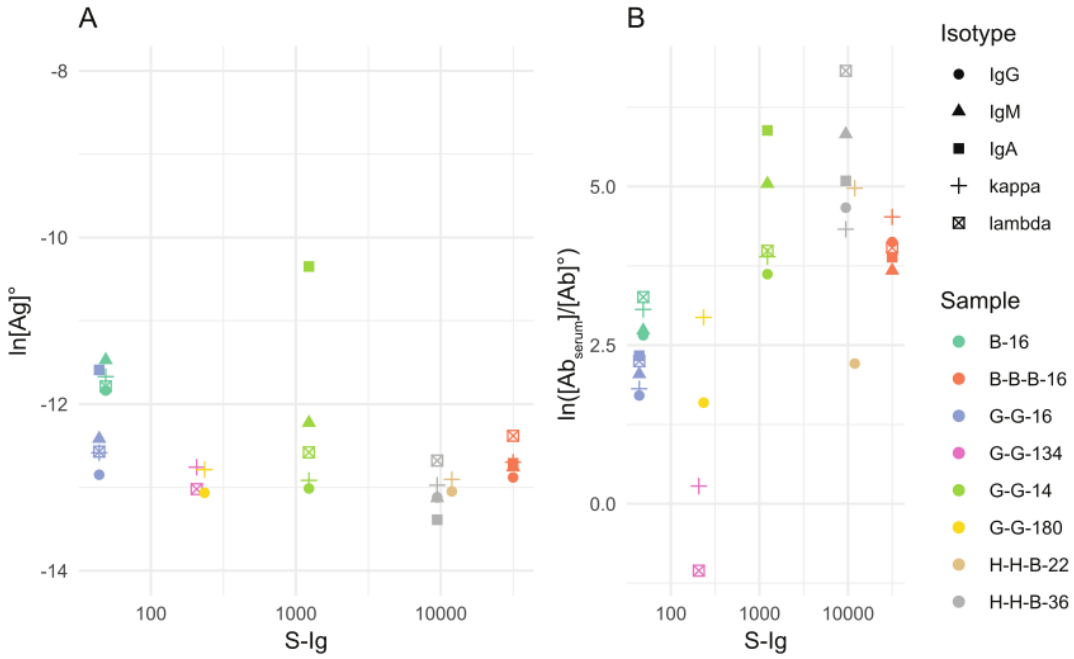
A
B
-8
-10
-12
-14
ln[Ag]°
100
1000
10000
S-Ig
5.0
2.5
0.0
ln([Ab$_{serum}$]/[Ab]°)
Isotype
IgG
IgM
IgA
kappa
lambda
Sample
B-16
B-B-B-16
G-G-16
G-G-134
G-G-14
G-G-180
H-H-B-22
H-H-B-36
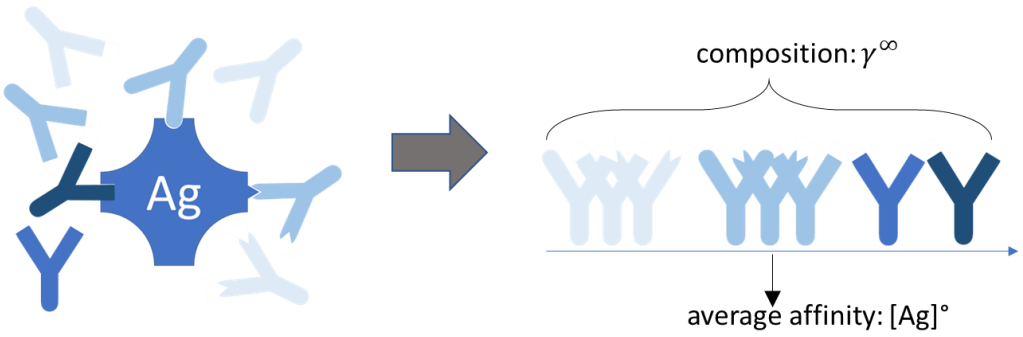
Figure 8.